Received: 30 June 2023 | Accepted: 3 July 2023

DOI: 10.1002/pamm.202300104

RESEARCH ARTICLE

Impact of soft magnetic α-Fe in hard $Nd_2Fe_{14}B$ magnetic materials: A micromagnetic study

Maximilian Reichel[1] | **Peter Groche**[2] | **Oliver Gutfleisch**[3] | **Jörg Schröder**[1]

[1]Institute of Mechanics, Faculty of Engineering, University of Duisburg-Essen, Essen, Germany

[2]Institute for Production Engineering and Forming Machines, Technical University Darmstadt, Darmstadt, Germany

[3]Functional Materials, Technical University Darmstadt, Darmstadt, Germany

Correspondence
Maximilian Reichel, Institute of Mechanics, Faculty of Engineering, University of Duisburg-Essen, Universitätsstraße 12, 45141 Essen, Germany.
Email: maximilian.reichel@uni-due.de

[Correction added on 08 September 2023, after first online publication: Projekt DEAL funding statement has been added.]

Funding information
German Research Foundation, Grant/Award Numbers: CRC/TRR 270, project A07, A01, A09

Abstract

The striving for the independence of fossil energy sources by further development of renewable energies as well as the change in mobility act as a driving force on technological innovations. Magnetic materials with improved magnetic efficiency help to push the limits for optimized, low-loss power conversion applications and electrification. Besides improving the chemical composition, that is, gaining better performance using alloys reduced or free of heavy rare earth elements, microstructure optimization has proven to be a crucial field of research. In order to better control the grain size, phase distribution and texture of the polycrystalline material, new process routes, such as severe plastic deformation, need to be investigated and explored in addition to the state-of-the-art method – sintering. Here, attention must be paid to the possible formation of soft magnetic α-Fe after the casting process prior to the actual deformation step, as these secondary phases negatively affect the hysteretic behavior of the magnet. Assistance in the analysis of the underlying magnetic mechanisms is provided by micromagnetic theory. Besides the reliable prediction of the magnetization distribution on micron-scale, especially in a multi-phase microstructure, it also allows for the analysis of the magnetic hysteresis behavior. This work provides a micromagnetic simulation frame work based on a finite element scheme. Relying on this framework the effective hysteresis behavior of two different heterogeneous microstructures ($Nd_2Fe_{14}B$ and $Nd_2Fe_{14}B/\alpha$-Fe) are analyzed and compared.

1 | INTRODUCTION

In general, magnets can be divided into soft and hard (permanent) magnetic materials. Soft magnets can be easily demagnetized by external magnetic fields, while hard magnets require particularly strong external fields for a zero net magnetization. H_c is better known as the material-dependent coercivity. This is also reflected in the characteristic of the magnetic hysteresis. While the soft magnetic hysteresis is in general very slender, corresponding to low values of coercive field strength, a hard magnetic hysteresis is usually very pronounced [1]. These fundamentally different material-dependent characteristics obviously lead to different areas of application. However, both types contribute to efficiency improvement of conversion equipment (transformers), power generators (wind turbines), sensors and electric motors for

E-mobility (electromobility), as presented in ref. [2]. Within this context the current challenges such as the transition from fossil to renewable energy supply or the change in mobility act as a driving force on technological innovations. To address these challenges, strong and particularly powerful high-performance magnets are required, cf. [2]. These high-performance magnets should ideally be made without heavy rare earth elements and consist mainly of earth abundant materials that are continuously accessible on the global market and produced under environmentally friendly mining conditions. In addition to the chemical composition, the microstructural texturing also has a major influence on the effective performance of the magnet [3]. As described in ref. [4], defect structures, such as non-magnetic inclusions, cracks or misoriented grains, in the grain structure have a negative influence on the overall performance of the material, that is, the prime figures of merit, summarized as extrinsic magnetic properties, M_r – remanent magnetization, H_c – coercivity and $(BH)_{max}$ – energy density, are reduced. In ref. [5] the influence of defect structures caused by strains acting on the surfaces of (Nd,Dy)-FeB core shell structures was investigated. The results are strongly diverging properties, significant discrepancies to the intrinsic magnetic properties, M_s – saturation magnetization and H_a – magnetocrystalline anisotropy, depending on the corresponding defect intensity. According to ref. [4] ideal sintered hard magnetic materials are a composition of ferromagnetic grains surrounded by a paramagnetic or non-magnetic phase. The ferromagnetic grains should ideally correspond to single domain particles with a strong uniaxial magneto-crystalline anisotropy and unified orientation direction, while the surrounding paramagnetic grain boundary phase acts as a layer for magnetic decoupling. The grain boundary is supposed to magnetically decouple the exchange interactions between the ferromagnetic grains. This prevents a premature magnetization reversal within the individual grains and therefore inhibits a cascade like demagnetization of the whole magnet, compare [6]. Currently, sintered magnets are considered to be the gold standard in the production of permanent magnets, even though the process involves many energetically expensive steps, cf. [7]. Here, novel processing routes based on severe plastic deformations (SPD) (e.g., the continuous rotary swaging process (CRS) [8]) or additive manufacturing (AM) (e.g., selected laser sintering (SLS) [9]) can be an option to tailor magnetic microstructures with enhanced effective, and in the case of additive manufacturing with local, magnetic properties. Developments of these processes strive for magnetically optimized, homogeneous micro-structures, although the process conditions are inhomogeneous on a microscopic level. Hence, a deeper understanding of the influence of fluctuations in the microscopic structures on the magnetic mechanisms is required. This can be extended with the help of numerical simulations. Here, we apply micromagnetic simulations based on the finite element method (FEM) are applied. Although the FEM is found to be numerically more expensive, compared to the finite difference method (FDM), its flexibility in discretizing heterogeneous microstructures provides a superior advantage, compare [10]. Micromagnetic simulations are applied nowadays in many applications to reveal magnetic interaction mechanisms, as the impact of exchange decouplings of grains [6], the influence of microstructural distortions [5, 11] or to analyze shape and size effects [12] on the critical magnetization reversal processes. A crucial challenge of micromagnetism is the conservation of the length of the magnetization vector $\boldsymbol{M} = M_s\boldsymbol{m}$, where M_s is the material-specific saturation magnetization and $\boldsymbol{m}$ represents the magnetic unit director. Here $||\boldsymbol{M}|| = M_s$ or $||\boldsymbol{m}|| = 1$ must hold for the entire simulation time. Since this unit constraint is not necessarily satisfied, different methods can be applied to restrict the magnetization to a constant length as, for example, renormalization techniques [13] or spherical coordinates [14], see also the incremental variational formulation [15]. A brief overview is given in ref. [16]. However, within this contribution a condensed perturbed Lagrange multiplier [17] is applied to computationally efficient enforce the unit constraint during simulations. The aim of the simulations considered here is to investigate the influence of soft magnetic α-Fe inclusions on the effective hysteresis property of an idealized permanent magnetic $Nd_2Fe_{14}B$ microstructure fabricated by the CRS technique. Hence this contribution proceeds as outlined below: *First*, the governing field equations and their corresponding boundary conditions are introduced. *Second*, the magnetic energy functional is presented. *Third*, the FE implementation of the introduced field equations presented. *Finally*, the considered boundary value problems are sketched and the simulation results are evaluated.

2 | FIELD EQUATIONS

Within this work, the focus is set on the analysis of purely magnetic phenomena, that is, mechanical or other types of stimuli on the magnetization behavior are neglected within the following contribution. Hence, the considered set of equations includes the magnetic Gauss law for the magnetostatic contributions while the Gilbert equation serves as the evolution equation of the magnetization vectors. The magnetic Gauss law for the magnetic field evolution reads as

$$\mathrm{div}\boldsymbol{B} = 0 \quad \text{with} \quad \boldsymbol{B} = \mu_0(\boldsymbol{H} + \boldsymbol{M}), \tag{1}$$

with $\boldsymbol{B}$ denoting the magnetic induction, that depends on the magnetic field $\boldsymbol{H}$ as well as the magnetization $\boldsymbol{M}$. The vacuum permeability is defined as μ_0. The magnetic field $\boldsymbol{H}$ is derived from the negative gradient of the potential φ as

$$\boldsymbol{H} := -\nabla\varphi. \tag{2}$$

A full description of the boundary value problem is possible due to the definition of the corresponding boundary conditions of the scalar potential φ on $\partial\mathcal{B} = \partial\mathcal{B}_\varphi \cup \partial\mathcal{B}_B$, with $\partial\mathcal{B}_\varphi \cap \partial\mathcal{B}_B = \emptyset$ as

$$\varphi = \varphi_0 \quad \text{on } \partial\mathcal{B}_\varphi \qquad \text{and} \qquad \boldsymbol{B}\cdot\boldsymbol{n} = \zeta_0 \quad \text{on } \partial\mathcal{B}_B. \tag{3}$$

The magnetic induction depends on the magnetic field as well as on the magnetization $\boldsymbol{m}(\boldsymbol{x}, t)$, that evolves over space and time. Hence, an evolution equation that captures the magnetization dynamics is required. In the context of micromagnetism, an appropriate method is the Gilbert equation of motion, which can be expressed as follows

$$\dot{\boldsymbol{m}} = -\gamma_0\mu_0\,\boldsymbol{m}\times\boldsymbol{H}^{\text{eff}} + \alpha\,\boldsymbol{m}\times\dot{\boldsymbol{m}}, \tag{4}$$

where $\dot{\boldsymbol{m}}$ denotes the rate of the magnetization vectors, γ_0 the gyromagnetic ratio, α defines the material-dependent Gilbert damping parameter and $\boldsymbol{H}^{\text{eff}}$ the so-called effective field. The effective field is not only the externally applied magnetic field, but unifies the contributions of the underlying crystal lattice and the magnetic exchange interaction. However, this will be explained in more detail in the next section. It should be noticed that the magnetization is only available within a magnetic solid $\mathcal{B}$ where it is defined as the relation $\boldsymbol{M} := M_s\,\boldsymbol{m}$. Outside the magnetic solid $\mathcal{B}$ the magnetization vanishes. A general assumption of most micromagnetic models is a constant operation temperature far below the Curie temperature, leading to the already mentioned length constraint of the magnetization vectors. In the context of the present work this constraint is enforced by applying a perturbed Lagrange multipler λ and a static condensation on element level to eliminate the computational drawback of the additional degree of freedom. This reads as

$$g_\lambda = \lambda\left(\left[||\boldsymbol{m}||^2 - 1\right] - \frac{\lambda}{2\kappa_L}\right), \tag{5}$$

where $\frac{\lambda^2}{2\kappa_L}$ is the source of the perturbation, leading to non-zero entries on the main diagonal of the system matrix enabling the static condensation. The parameter κ_L is of pure numerical nature and assumed to be $\sim 10^5$.

3 | ENERGY FUNCTIONAL

A precise description of the magnetization behavior within magnetic solids requires the knowledge of the most important competing energy contributions. Here, these internal and external energies are unified within the functional

$$\mathcal{H}(\boldsymbol{H}, \boldsymbol{m}, \nabla\boldsymbol{m}) = \mathcal{H}^{\text{mag}}(\boldsymbol{H}, \boldsymbol{m}) + \mathcal{H}^{\text{exc}}(\nabla\boldsymbol{m}) + \mathcal{H}^{\text{ani}}(\boldsymbol{m}), \tag{6}$$

where $\mathcal{H}^{\text{mag}}$ denotes the magnetostatic energy, that considers internal (stray/demagnetizing) and external magnetic fields, the magnetic exchange energy $\mathcal{H}^{\text{exc}}$ estimates the interaction between the magnetic moments, and the magneto crystalline anisotropy $\mathcal{H}^{\text{ani}}$ captures the energetic contribution from the crystal lattice. In this particular case it is a uniaxial anisotropy contribution. Those energies can be derived as

$$\begin{aligned} \mathcal{H}^{\text{mag}}(\boldsymbol{H}, \boldsymbol{m}) &= -\frac{1}{2}\mu_0\,\boldsymbol{H}\cdot\boldsymbol{H} - \mu_0 M_s \boldsymbol{H}\cdot\boldsymbol{m} \\ \mathcal{H}^{\text{exc}}(\nabla\boldsymbol{m}) &= A^{\text{exc}}\nabla\boldsymbol{m} : \nabla\boldsymbol{m}, \quad \text{and} \quad \mathcal{H}^{\text{ani}}_{\text{uni}}(\boldsymbol{m}) = K^{\text{ani}}_{\text{uni}}(\boldsymbol{m}\cdot\boldsymbol{a}), \end{aligned} \tag{7}$$

where A_{exc} denotes the exchange coefficient, $K^{\text{ani}}_{\text{uni}}$ the anisotropy parameter and $\boldsymbol{a} = [\sin\theta_1\cos\theta_2, \sin\theta_1\sin\theta_2, \cos\theta_1]^T$ a structural vector indicating the preferred/easy-axis of the material. The magnetization vectors will be subject to a torque

developed by the so-called effective field [18], that is derived via the variational derivative of $\mathcal{H}$ w.r.t. the magnetization $\boldsymbol{m}$ as

$$\boldsymbol{H}^{\text{eff}} = \delta_{\boldsymbol{m}}\mathcal{H} = \frac{-1}{\mu_0 M_s}[\boldsymbol{\pi} - \operatorname{div}\boldsymbol{\Pi}], \quad \text{with} \quad \boldsymbol{\pi} = \frac{\partial\,\mathcal{H}}{\partial\,\boldsymbol{m}} \quad \text{and} \quad \boldsymbol{\Pi} = \frac{\partial\,\mathcal{H}}{\partial\,\nabla\boldsymbol{m}} \tag{8}$$

and unifies the contributions of the magnetostatic fields, the exchange interactions between the magnetization vectors and the influence of the underlying crystal lattice of the considered material.

4 | FINITE ELEMENT FORMULATION

This section presents the weak forms needed to implement the formulation into a finite element frame work. These are based on the differential equations introduced in Section 2. Since the formulations considered here lead to very complicated derivations and complex systems of equations, the weak forms are implemented into AceGen/AceFEM [19], which possesses a strong automatic differentiation engine. A general overview of the FEM is provided in ref. [20]. The considered weak forms yield

$$\begin{aligned}
G_\varphi &= -\int_{\mathcal{B}} \delta\boldsymbol{H}\cdot\boldsymbol{B}\,\mathrm{dv} + \int_{\partial\mathcal{B}} \delta\varphi\,\zeta_0\,\mathrm{da}\\
G_m &= \int_{\mathcal{B}} \Big[\delta\boldsymbol{m}\cdot(\dot{\boldsymbol{m}} - \alpha\,\boldsymbol{m}\times\dot{\boldsymbol{m}} - \boldsymbol{m}\times\partial_{\boldsymbol{m}}\mathcal{H}) - 2A_{\text{exc}}\sum_{i=1}^{3}\nabla\delta m_i\cdot(\boldsymbol{m}\times\nabla m_i)\Big]\,\mathrm{dv} + \int_{\mathcal{B}} 2\,\delta\boldsymbol{m}\cdot\boldsymbol{m}\,\lambda\,\mathrm{dv}\\
G_\lambda &= \int_{\mathcal{B}} \delta\lambda\left(||\boldsymbol{m}||^2 - 1 - \frac{\lambda}{\kappa_L}\right)\mathrm{dv}
\end{aligned} \tag{9}$$

where $\delta\varphi, \delta\boldsymbol{H}, \delta\boldsymbol{m}$ and $\delta\nabla\boldsymbol{m}$ denote the variational counterparts of the primary variables and their spatial derivatives and $\dot{\boldsymbol{m}}$ the time derivative of the magnetization. The additional degree of freedom, that is, the Lagrange multiplier is eliminated within the finite element formulation utilizing to a static condensation on element level, as presented in ref. [20] for typical engineering problems and in ref. [17] for a micromagnetic application.

5 | ANALYSIS OF MAGNETIZATION REVERSAL IN HETEROGENEOUS MICROSTRUCTURES

In this section, two different scenarios for microstructural compositions of $Nd_2Fe_{14}B$ magnets are considered. Thereby, the special focus of this case study is on the influence of α-Fe impurities on the effective hysteresis properties of permanent magnetic materials. α-Fe is a soft phase material that forms during the casting process typically in the morphology of large dendritic grains within the $Nd_2Fe_{14}B$ matrix grains and excess Nd-rich phases (the latter being paramagnetic). Upon homogenization these phases recombine to form more $Nd_2Fe_{14}B$ matrix grains and eliminate Fe. Soft magnetic materials have significantly lower resistance to external magnetic fields compared to permanent magnetic materials, resulting in significantly lower coercivity. Since the α-Fe is in direct contact with the hard magnetic $Nd_2Fe_{14}B$ phase (no separation of both materials by a paramagnetic grain boundary phase), it initiates a premature reversal within the magnetically harder part of the magnet. The result is a significantly lower coercivity of this magnet, compared to a magnet with no impurities. In the following, a grain composition without α-Fe impurities is considered, see Figure 1. It consists of seven ferromagnetic grains with the material properties of $Nd_2Fe_{14}B$, that is, exchange constant $A_{\text{exc}} = 8.0 \cdot 10^{-12}$ J/m, saturation magnetization $M_{\text{s}} = 1.432 \cdot 10^6$ A/m and magneto crystalline anisotropy $K_1 = 4.9 \cdot 10^6$ J/m^3 [21]. The grains are assumed to have a diameter of 500 nm (doubles the single domain particle size of $Nd_2Fe_{14}B$ ~200–300 nm [22]), and are assumed to be magnetically decoupled from each other by a 5-nm-thick paramagnetic Nd-rich grain boundary. The whole microstructure corresponds to the diameter $d_{\text{tot}} = 1350$ nm.

Since so-called stray fields form around magnetic materials, which can strongly influence the properties of the magnet, these must also be considered in the simulation. This implies that the influence of the outer space region has to be

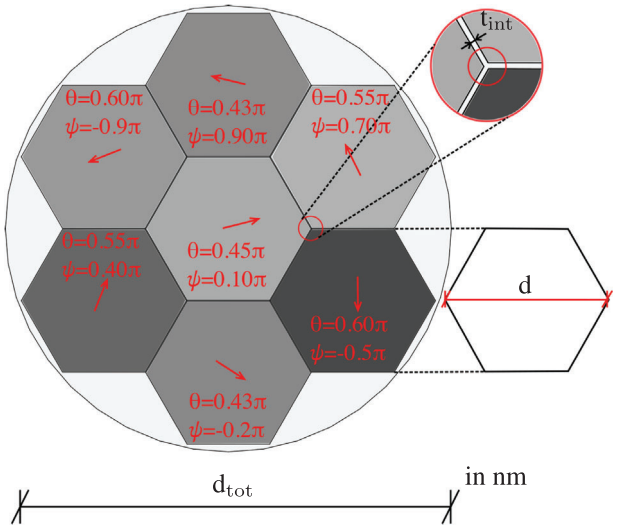

FIGURE 1 An idealized $Nd_2Fe_{14}B$ microstructure consisting of seven hexagonal grains of diameter $d = 500$ nm which are magnetically decoupled from each other by a paramagnetic grain boundary ($t_{int} = 5$ nm). The easy-axis of anisotropy can be expressed by the corresponding angles and spherical coordinates.

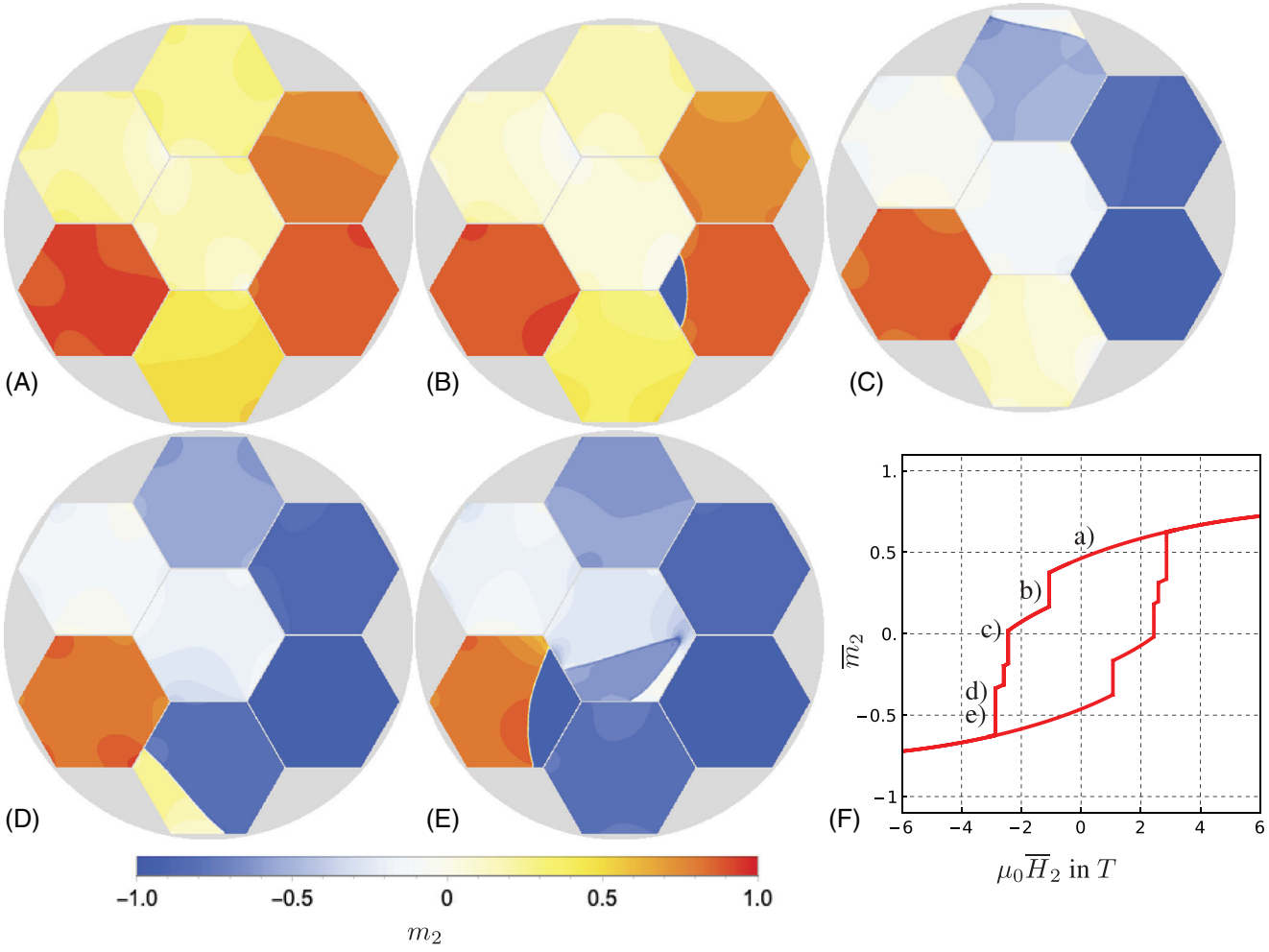

FIGURE 2 The evolution of the magnetization reversal is presented with in (A) – (E). Starting with (A) the magnetization vectors are aligned parallel to the easy-axis of the individual grains. Decreasing the field strength leads to (B) nucleation within the corners of the grains and (C) eventually initiating their cascade like magnetization reversal. Further decreasing the external magnetic field to the maximal applied field strength of $\mu_0 \boldsymbol{H} = -6\,T$ reverses all grains into the corresponding direction. This switching behavior is depicted in (F) as a hysteresis loop.

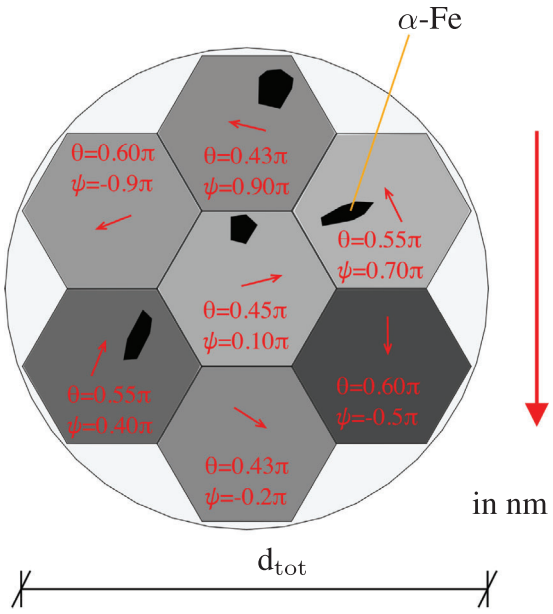

FIGURE 3 α-Fe impurities are added to the idealized seven grain $Nd_2Fe_{14}B$ microstructure. Between the α-Fe impurities and the $Nd_2Fe_{14}B$ grains no separating boundary exists.

considered discretely as well. In order to capture this numerically as efficiently as possible, the method presented in ref. [23] for the consideration of the outer space is applied in this work. To obtain a typical hysteresis loop and evaluate the effective magnetic behavior, an alternating external magnetic field $\mu_0\overline{\boldsymbol{H}} = [0, 6, 0]^T$ T is applied. In the simulated hysteresis loop (Figure 2F) several kinks can be seen. These result from the different switching times due to different orientations of the individual decoupled grains. The grain boundary prevents reversal from one switching grain to another and thus premature reversal. It is also clear from Figure 2F that the coercivity of the magnet under consideration is ~3 T. An improvement of this property can be achieved mainly by a better alignment of the easy-axis of the grains. A fabrication such that the easy-axis of the individual grains are oriented (with slight variations) in one direction can lead to a more rectangular hysteresis due to a later nucleation within the grains. The reversal process shown in Figure 2A–E also shows the separate switching of the individual grains. In each case, nucleation begins in the corners of the grains. Subsequently, the reversal propagates cascade-like through the grain, leading to the characteristic kinks in the hysteresis. In the case of impurified microstructures, however, the behavior may be different. To investigate this in more detail, the boundary value problem introduced in Figure 1 is extended to contain α-Fe impurities in the following example.

The modified boundary value problem with soft magnetic inclusions can be found in Figure 3. Here, local impurities are taken into account by defining additional regions within the permanent magnetic grains and assigning soft magnetic properties such that the material response of α-Fe can be simulated. The following material properties of α-Fe are taken from ref. [13]: exchange constant $A_{\text{exc}} = 1.0 \cdot 10^{-12}$ J/m, saturation magnetization $M_{\text{s}} = 5 \cdot 10^6$ A/m and magneto crystalline anisotropy $K_1 = 4 \cdot 10^4$ J/m^3 and $K_2 = 6 \cdot 10^3$ J/m^3. The hysteresis loop is obtained by applying the same alternating external magnetic field $\mu_0\overline{\boldsymbol{H}} = [0, 6, 0]^T$ T to the microstructure presented in Figure 3. The resulting hysteresis loop is about 10 times more slender compared to the previously simulated loop (Figure 2F). The reason for this behavior can be identified as the direct contact of the soft magnetic material with the permanent magnetic grain. Since the α-Fe impurities have a significantly lower resistance (coercivity) to opposing external magnetic fields, nucleation starts at these spots. Due to the fact that impurities collect at random locations within the grain matrix during the manufacturing process, grain boundaries between the inclusions and the actual grain are missing. As a result, soft and permanent magnetic materials are in direct contact with each other, that is, they are not exchange decoupled. After the reversal of the soft magnetic region (Figure 4B), this leads to a fast transition of the reversal to the permanent magnetic material (Figure 4C) and thus to a premature switching of the entire grain (Figure 4E). A comparison of the simulation results with the findings from ref. [11] gives rise to further analysis, since here α-Fe phase inclusions about 100 nm in size appear to couple effectively. However, the microstructures were different there.

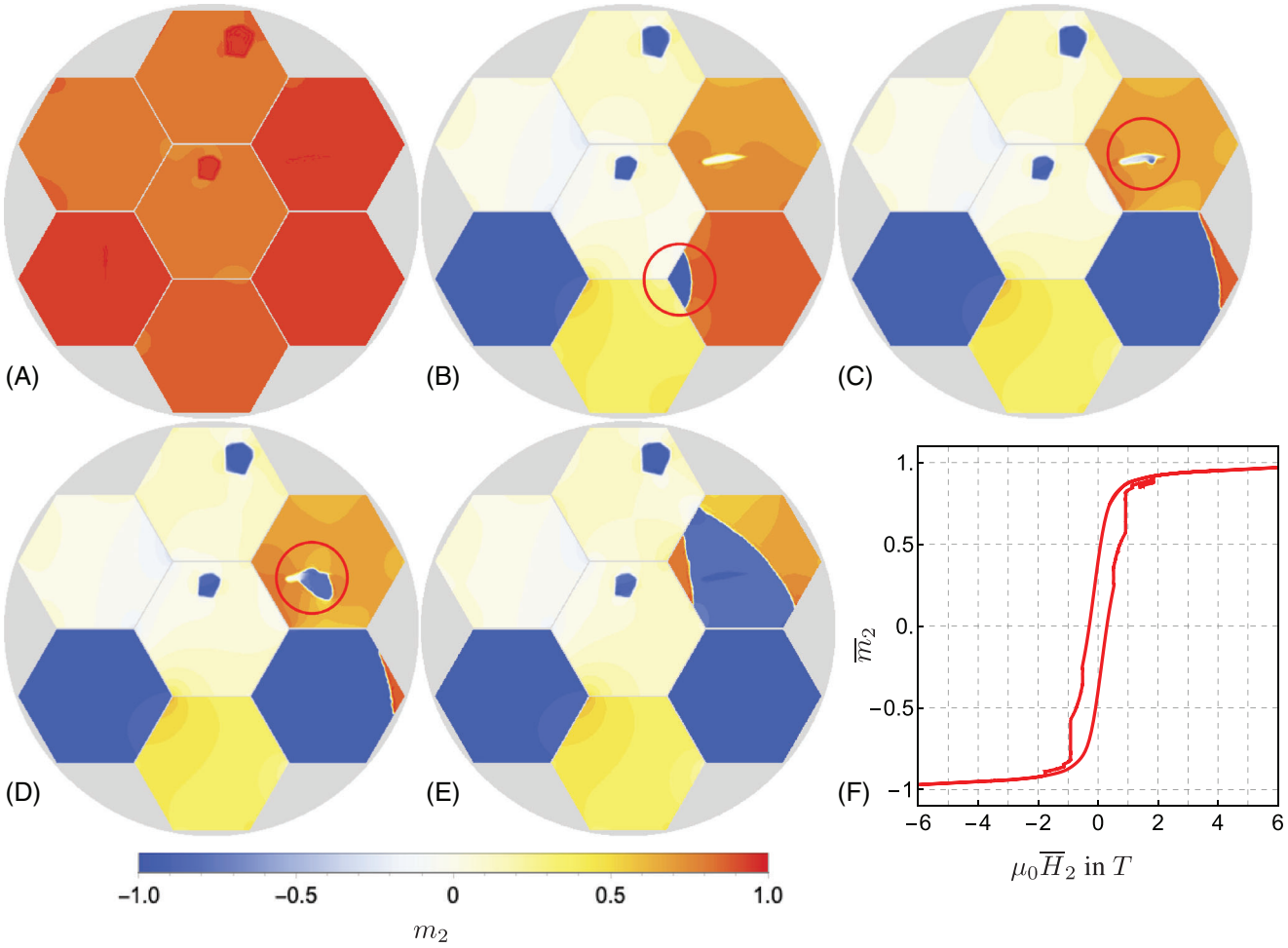

FIGURE 4 The evolution of the magnetization reversal is presented with in (A) – E). (A) shows the full magnetization of the microstructure along the x_2-axis. (B) highlights the nucleation of a homogeneous grain, that is, no α-Fe contamination, at a triple junction of the grain boundary. After the reversal of the α-Fe contamination in (B), the reversal "jumps over" to the permanet magnetic grain in (C) and propagates through it in (D) – (E). This switching behavior is depicted in (F) as a hysteresis loop.

6 | CONCLUSION

This work deals with the influence of soft magnetic inclusions in a permanent magnetic grain matrix on the effective magnetization behavior. Using an idealized microstructure, the effective properties in form of the hysteresis loop of a perfectly decoupled magnet and a magnet degraded by α-Fe inclusions were compared. It has been shown that the inclusions lead to a premature reversal of the respective inhomogeneous grains. In the case of several contaminated grains, this leads to a severe decrease in the coercivity and squareness in the second quadrant. From a technological point of view, the results clearly indicate the necessity of a heat treatment in order to reach an acceptable level of coercivity when casted (Nd,Dy)-FeB is the starting point of a process chain. In subsequent studies, different impact factors, such as non-magnetic inclusions or distortions, on the magnetic properties will be investigated.

ACKNOWLEDGMENTS

We gratefully acknowledge the financial support of the German Research Foundation (DFG) in the framework of the CRC/TRR 270, project A07 "Scale-bridging of magneto-mechanical mesostructures of additive manufactured and severe plastically deformed materials", and also A01 and A09 projects therein, project number 405553726.

Open access funding enabled and organized by Projekt DEAL.

REFERENCES

1. Inoue, A., & Kong, F. (2020). Soft magnetic materials. *Encyclopedia of Smart Materials*, *5*, 10–23.
2. Gutfleisch, O., Willard, M. A., Brück, E., Chen, C. H., Sankar, S. G., & Ping Liu, J. (2011). Magnetic materials and devices for the 21st century: Stronger, lighter, and more energy efficient. *Advanced Materials*, *23*, 821–842. https://doi.org/10.1002/adma.201002180
3. Woodcock, T. G., Zhang, Y., Hrkac, G., Ciuta, G., Dempsey, N., Schrefl, T., Gutfleisch, O., & Givord, D. (2012). Understanding the microstructure and coercivity of high performance NdFeB-based magnets. *Scripta Materialia*, *67*, 536–541. https://doi.org/10.1016/j.scriptamat.2012.05.038
4. Kronmüller, H. (1987). Theory of nucleation fields in inhomogeneous ferromagnets. *Physica Status Solidi (b)*, *144*, 385–396. https://doi.org/10.1002/pssb.2221440134
5. Helbig, T., Loewe, K., Sawatzki, S., Yi, M., Xu, B. X., & Gutfleisch, O. (2017). Experimental and computational analysis of magnetization reversal in (Nd,Dy)-Fe-B core shell sintered magnets. *Acta Materialia*, *127*, 498–504. https://doi.org/10.1016/j.actamat.2017.01.055
6. Soderžnick, M., Sepehri-Amin, H., Sasaki, T. T., Ohkubo, T., Takada, Y., Sato, T., Kaneko, Y., Kato, A., Schrefl, T., & Hono, K. (2017). Magnetization reversal of exchange-coupled and exchange-decoupled Nd-Fe-B magnets observed by magneto-optical Kerr effect microscopy. *Acta Materialia*, *135*, 68–76. https://doi.org/10.1016/j.actamat.2017.05.006
7. Brown, D., Ma, B.-M., & Chen, Z. (2002). Developments in the processing and properties of NdFeB-type permanent magnets. *Journal of Magnetism and Magnetic Materials*, *248*, 432–440. https://doi.org/10.1016/S0304-8853(02)00334-7
8. Chi, F.Wießner, L., Gröb, T., Bruder, E., Sawatzki, S., Löwe, K., Gassmann, J., Müller, C., Durst, K., Gutfleisch, O., & Groche, P. (2019). Towards manufacturing of Nd-Fe-B magnets by continuous rotary swaging of cast alloy. *Journal of Magnetism and Magnetic Materials*, *490*, 165405. https://doi.org/10.1016/j.jmmm.2019.165405
9. Yang, Y., Ragnvaldsen, O., Bai, Y., Yi, M., & Xu, B.-X. (2019). 3D non-isothermal phase-field simulation of microstructure evolution during selective laser sintering. *npj Computational Materials*, *5*, 81. https://doi.org/10.1038/s41524-019-0219-7
10. Vansteenkiste, A., Leliaert, J., Dvornik, M., Helsen, M., Garcia-Sanchez, F., & Van Waeyenberge, B. (2014). The design and verification of MuMax3. *AIP Advances*, *4*, 107133. https://doi.org/10.1063/1.4899186
11. Sepehri-Amin, H., Dirba, I., Tang, X., Ohkubo, T., Schrefl, T., Gutfleisch, O., & Hono, K. (2019). Development of high coercivity anisotropic Nd-Fe-B/Fe nanocomposite powder using hydrogenation disproportionation desorption recombination process. *Acta Materialia*, *175*, 276–285. https://doi.org/10.1016/j.actamat.2019.06.017
12. Fischbacher, J., Kovacs, A., Gusenbauer, M., Oezelt, H., Exl, L., Bance, S., & Schrefl, T. (2018). Micromagnetics of rare-earth efficient permanent magnets. *Journal of Physics D: Applied Physics*, *51*, 193002. https://doi.org/10.1088/1361-6463/aab7d1
13. Sridhar, A., Keip, M. A., & Miehe, C. (2016). Homogenization in micro-magneto-mechanics. *Computational Mechanics*, *58*, 151–169. https://doi.org/10.1007/s00466-016-1286-y
14. Dornisch, W., Schrade, D., Xu, B.-X., Keip, M.-A. & Müller, R. (2018). Coupled phase field simulations of ferroelectric and ferromagnetic layers in multiferroic heterostructures. *Archive of Applied Mechanics*, *89*, 1031–1056. https://doi.org/10.1007/s00419-018-1480-9
15. Miehe, C., & Ethiraj, G. (2012). A geometrically consistent incremental variational formulation for phase field models in micromagnetics. *Computer Methods in Applied Mechanics and Engineering*, *245-246*, 331–347. https://doi.org/10.1016/j.cma.2012.03.021
16. Reichel, M., Xu, B.-X., & Schröder, J. (2022). A comparative study of finite element schemes for micromagnetic mechanically coupled simulations. *Journal of Applied Physics*, *132*, 183903. https://doi.org/10.1063/5.0105613
17. Reichel, M., Schröder, J., & Xu, B.-X. (2023). Efficient micromagnetic finite element simulations using a perturbed Lagrange multiplier method. *Proceedings in Applied Mathematics and Mechanics*, *22*, e202200016. https://doi.org/10.1002/pamm.202200016
18. Schrefl, T., & Fidler, J. (1998). Modelling of exchange-spring permanent magnets. *Journal of Magnetism and Magnetic Materials*, *177-181*, 970–975. https://doi.org/10.1016/S0304-8853(97)00653-7
19. Korelc, J., & Wriggers, P. (2016). *Automation of finite element method*. Springer. https://doi.org/10.1007/978-3-319-39005-5
20. Wriggers, P. (2008). *Nonlinear finite element methods*. Springer Science & Business Media. https://doi.org/10.1007/978-3-540-71001-1
21. Coey, J. M. D. (2010). *Magnetism and magnetic materials*. Cambridge University Press. https://doi.org/10.1017/CBO9780511845000
22. Gutfleisch, O. (2000). Controlling the properties of high energy density permanent magnetic materials by different processing routes. *Journal of Physics C: Applied Physics*, *33*, R157–R172. https://doi.org/10.1088/0022-3727/33/17/201
23. Schröder, J., Reichel, M., & Birk, C. (2022). An efficient numerical scheme for the FE-approximation of magnetic stray fields in infinite domains. *Computational Mechanics*, *70*, 141–153. https://doi.org/10.1007/s00466-022-02162-1

How to cite this article: Reichel, M., Groche, P., Gutfleisch, O., & Schröder, J. (2023). Impact of soft magnetic α-Fe in hard $Nd_2Fe_{14}B$ magnetic materials: A micromagnetic study. *Proceedings in Applied Mathematics and Mechanics*, *23,* e202300104. https://doi.org/10.1002/pamm.202300104